ACS OMEGA

Open Access

http://pubs.acs.org/journal/acsodf

Article

New Process for Na_2CO_3 Production from Na_2SO_4 Based on Modeling the Na_2SO_4–$(NH_4)_2SO_4$–MEA–MEG–H_2O System

Binghui Li, Edouard Asselin,* and Zhibao Li*

Cite This: *ACS Omega* 2024, 9, 1265–1277

Read Online

ACCESS | Metrics & More | Article Recommendations

ABSTRACT: Alternative means for soda ash (Na_2CO_3) production from sodium sulfate (Na_2SO_4) are needed due to the intensive consumption of energy in the conventional Mirabilite-Solvay process (MSP). We demonstrate a new process to produce soda ash using sodium sulfate as a feed material. The new process relies on the antisolvent crystallization of unreacted Na_2SO_4 to separate it from soluble $(NH_4)_2SO_4$ in a mixed monoethanolamine (MEA) and monoethylene glycol (MEG) solution. To develop the process, the solubilities of Na_2SO_4 and $(NH_4)_2SO_4$ solids in aqueous mixed MEA–MEG solutions were first measured and then modeled using regressed paired-ion interactions from the electrolyte nonrandom two-liquid (E-NRTL) model. Anhydrous dense soda ash with a bulk density of up to 1146 kg/m^3 was obtained when the concentrated Na_2SO_4 brines reacted with CO_2 and NH_3.

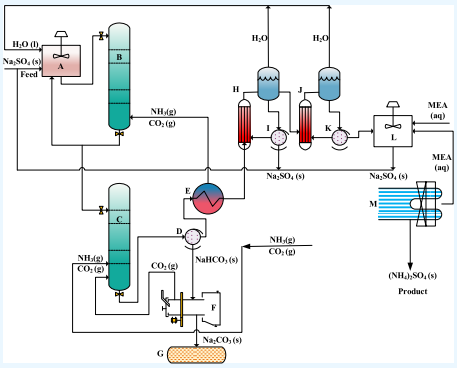

1. INTRODUCTION

Sodium sulfate (Na_2SO_4) is the second most common water-soluble mineral, with only sodium chloride (NaCl) being more abundant.[1] Quantitatively, the U.S. Geological Survey[2] reports a total world production of natural sodium sulfate to be approximately 8 million tons per annum. Although its uses are in detergents, glass, pulp and paper, textiles, and carpet fresheners, world consumption has remained stagnant in recent years. Sodium sulfate is not only the second largest in terms of reserves, but also one of the two most important feedstocks, alongside sodium chloride, for Na_2CO_3 production. The demand for dense Na_2CO_3 continues to grow, with a total production of 55 million metric tons in 2018 and a projected 10 million metric tons increase within a decade.[3−5] The two most prominent processes[6−10] to produce dense Na_2CO_3 include the Solvay process, which uses sodium chloride (brine solution) as a feed, and the Trona process, which mines crude soda from deposits for later purification. The former process consists of limestone calcination to generate CO_2, and CO_2 absorption into ammoniated brine to make sodium bicarbonate, which precipitates from the solution, followed by filtration and eventually calcination of the bicarbonate. Ammonia is recovered through distillation and a product liquor containing a large quantity of suspended solids with high chloride content is generated, which is very detrimental to the environment if not properly treated. The Trona process depends on the mining of trona deposits or salt lakes that contain basic Na_2CO_3. The United States possesses the largest deposits of trona and numerous carbonate-rich brine lakes;[1] it is the main soda ash producer that uses this method, but the dependency on a natural resource limits Trona's application in other countries. Both the Solvay and Trona processes involve highly intensive energy-consuming steps such as high-temperature calcination and roasting, which justifies seeking greener and more economically friendly methods.

Sodium sulfate is a promising substitute for sodium chloride as a feedstock for dense Na_2CO_3 production, but this idea is not new. According to Garrett's sodium sulfate handbook,[1] the use of sodium sulfate for Na_2CO_3 production goes back to the ancient Egyptian period where it was produced in a process analogous to the first noted industrial method: the Leblanc process, which used sodium sulfate to produce Na_2CO_3 at a large scale during the Industrial Revolution. Although the emergence of the more economical Solvay process rendered the Leblanc process obsolete, the Leblanc process was the standard for Na_2CO_3 production using a Na_2SO_4 feed. The latter was actually obtained from sodium chloride through the Mannheim process. The major reactions involved in the Leblanc process are

$$Na_2SO_4 + 2C \rightarrow Na_2S + 2CO_2 \ (T = 1000\ ^\circ C) \quad (1)$$

$$Na_2S + CaCO_3 \rightarrow Na_2CO_3 + CaS \quad (2)$$

Received: September 29, 2023
Revised: November 15, 2023
Accepted: November 17, 2023
Published: December 26, 2023

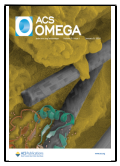

Shown in Figure 1, in contrast to the Leblanc process, which is also referred to as the pyrolysis method, a wet process, also

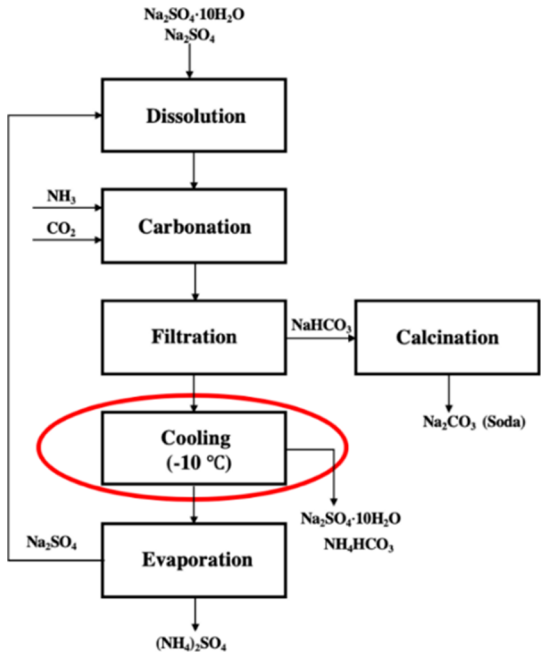

Figure 1. Conventional Mirabilite-Solvay Process (MSP).

referred to as the Mirabilite-Solvay process (MSP), was developed in Russia in the early 1950s and was later tested on a pilot scale by some Canadian operators.[1] In this process, Na_2CO_3 is obtained as well as byproduct $(NH_4)_2SO_4$. The main reaction is provided below:

$$Na_2SO_4 + 2NH_3 + 2CO_2 + 2H_2O \rightarrow 2NaHCO_3 \downarrow + (NH_4)_2SO_4 \quad (3)$$

Following the dissolution of Na_2SO_4, it is carbonated via reaction 3, where the purified brines are pumped into a tower with NH_3 and CO_2 gas addition followed by the filtration and calcination of bicarbonate. The calcination step converts the bicarbonate to Na_2CO_3. In order to achieve the recycling of unreacted Na_2SO_4, and to obtain the byproduct $(NH_4)_2SO_4$, a multistep, highly energy-intensive separation process is required. Cisternas et al.[11] pointed out that the $Na_2SO_4-(NH_4)_2SO_4-H_2O$ system forms the double salt $Na_2SO_4\ (NH_4)_2SO_4\ 4H_2O$ at 298 K, but does not form double salts at 333 K, meaning that the Na_2SO_4 may precipitate as the decahydrate at 298 K, and in the anhydrous form at 333 K. In practice, the filtrate from $NaHCO_3$ separation has to be cooled down to as low as 263 K to obtain $Na_2SO_4\ 10H_2O$, then the filtrate is subjected to evaporation to separate more Na_2SO_4, followed by cooling crystallization for $(NH_4)_2SO_4$. Furthermore, during the reaction of ammonia gas with the Na_2SO_4 brine, fixed ammonia (ammonium sulfate) is produced as a product for sale, while ammonia gas is consumed and unrecyclable. This impedes the use of the wet process in places with scarce or expensive ammonia.

Rather than the standard methods discussed above, $Na_2SO_4-(NH_4)_2SO_4$ separation via organic (anti)solvent crystallization should be considered because of its high efficiency and provided that an adequate water-miscible solvent is selected. Oosterhof et al.[12] successfully used mono ethylene glycol (MEG) as an antisolvent during evaporative crystallization to produce anhydrous Na_2CO_3 at atmospheric pressure. This is because the addition of ethylene glycol to Na_2CO_3 solution deceases the transition temperature of the Na_2CO_3 monohydrate to anhydrous transformation. Instead of MEG, Wang and Li[8] found that $NaHCO_3$ can be completely transformed into Na_2CO_3 at only 353 K in an aqueous solution containing at least 65 wt % of monoethanolamine (MEA) which is often used for CO_2 capture.[13,14] Our recently published study[15] reported that the solubility of Na_2SO_4 sharply decreases with increasing MEA concentration while the solubility of $(NH_4)_2SO_4$ progressively increases. This finding hints at the possibility of using MEA to salt out Na_2SO_4 in order to accomplish its separation from $(NH_4)_2SO_4$. Experimental results obtained in our laboratory revealed that Na_2SO_4 can be completely recovered from the $NaHCO_3$ separation filtrate when a 50 wt % MEA aqueous solution is used at 353.15 K. The $(NH_4)_2SO_4$ can also be fully recovered using cooling evaporative crystallization. These experiments showed that MEA, acting as a crystallization solvent, has a good separation effect on sodium sulfate and ammonium sulfate, but we found that the color of the MEA solution darkened and degraded at a relatively high temperature and high concentration. Another unfavorable side effect was the fact that $(NH_4)_2SO_4$ partially undergoes the following decomposition reaction in the presence of MEA, thus releasing ammonia gas:

$$(NH_4)_2SO_4 \xrightarrow[\Delta]{MEA} NH_3 \uparrow + NH_4HSO_4 \quad (4)$$

This decomposition leads to ammonia emissions and an increase in the concentration of ammonium bisulfate in solution, which not only affects the production environment but also makes it difficult to crystallize the ammonium sulfate due to an increase in its overall solubility.

In order to avoid high concentrations of MEA in solution, which are known to be corrosive to process equipment during the carbon dioxide capture process, monoethylene glycol (MEG) can be added as a vapor reduction additive (VRA).[16,17] This reduces the amine vapor pressure, causing the vaporization of the MEA solvent in the desorption step, resulting in less heat in the reboiler. Puxty et al.[17] evaluated ten cosolvents and found that a 31% reduction in vapor pressure was achieved at a 30 wt % MEG concentration in the absorbent solution. However, it is rarely reported in the literature that mixed MEA and MEG solutions (cosolvents) could be applied as antisolvents to accomplish the separation of sulfate salts with the help of crystallization techniques.

Solid−liquid equilibria of Na_2SO_4 and $(NH_4)_2SO_4$ in an aqueous mixture of MEA and MEG play an important role in the design and engineering scale-up of their crystallization separation. Neerup et al.[18] determined the solubility of ice and urea in two systems: urea−MEA−H_2O and MEG−MEA−H_2O for the improvement of thermodynamic modeling of new CO_2 solvents. The Pitzer−Lorimer approach[19] was recently used to correlate eight salts' solubility data in water−MEG mixtures with adequate results. The mixed-solvent electrolyte (MSE) model[20,21] developed by OLI Systems was used to successfully model phase equilibria for the mixed MEG electrolyte systems, which contain various salts and dissolved gases.

The remainder of this article is laid out as follows: we describe in detail our proposed production process for Na_2CO_3 from Na_2SO_4. Then, we introduce new measurements of solubility data for Na_2SO_4 and $(NH_4)_2SO_4$ in a mixed MEG−MEA aqueous solution, as well as progress toward a thermodynamic

https://doi.org/10.1021/acsomega.3c07533
ACS Omega 2024, 9, 1265−1277

model for the Na_2SO_4−$(NH_4)_2SO_4$−MEG−MEA−H_2O system using the E-NRLT activity coefficient model. The mixed MEG−MEA antisolvent crystallization for the separation of Na_2SO_4 and $(NH_4)_2SO_4$ salts is then tested to evaluate the feasibility of the proposed process.

2. MATERIALS AND METHODS

2.1. Materials and Reagents. The reagent-grade Na_2SO_4, $(NH_4)_2SO_4$, NH_4HSO_4, $(NH_4)_2CO_3$, $CaCO_3$, NH_4HCO_3, HCl, and monoethanolamine (MEA) were all purchased from XiLong Scientific Company, China. Monoethylene glycol (MEG) and gypsum were provided by Shanghai Macklin Biochemical Co., Ltd. The listed reagents in Table 1 were used as commercially purchased without further purification unless otherwise stated. Prior to measurements being taken, each individual piece of equipment was fully rinsed with DI water and thoroughly dried.

Table 1. List of Chemical Reagents Used in This Study

chemical compound	formula	supplier	analytical purity
sodium sulfate	Na_2SO_4	XiLong Scientific Company, China	≥99.5%
ammonium bicarbonate	NH_4HCO_3	ibid	21−22% NH_3 basis
monoethanolamine (MEA)	C_2H_7NO	ibid	≥99%
monoethylene glycol (MEG)	$C_2H_6O_2$	Shanghai Macklin Biochemical Co., Ltd., China	≥99%
ammonium sulfate	$(NH_4)_2SO_4$	XiLong Scientific Company, China	≥99%
ammonium bisulfate	NH_4HSO_4	ibid	≥99%
calcium sulfate dihydrate	$CaSO_4{\cdot}2H_2O$	Shanghai Macklin Biochemical Co., Ltd., China	≈95%
ammonium carbonate	$(NH_4)_2CO_3$	XiLong Scientific Company, China	≥99%
calcium carbonate	$CaCO_3$	ibid	≥99%
hydrochloride acid	HCl	ibid	35−37%

2.2. Material Characterization. Slurry samples of Na_2SO_4 and $(NH_4)_2SO_4$ crystallized from the MEA−MEG cosolvent solution were taken from the reactor at a given retention time and immediately filtered through 0.22 μm Millipore Swinnex filters. The recovered crystals were dried after filtration and stored in test tubes for further analysis. SEM images of the obtained crystals were measured with a JSM-7610F (JEOL Ltd., Japan) while crystal phases were characterized by Empyrean X-ray diffraction (XRD) analysis (PANalytical B.V., Netherland). All reported values are the result of at least duplicate experiments.

2.3. Proposed Process Description. In Figure 2, we present a novel process that effectively separates Na_2SO_4 and $(NH_4)_2SO_4$. If required, ammonia gas recycling is accomplished by the decomposition of ammonium sulfate using low-grade limestone ($CaCO_3$),[22−24] in which alpha-type calcium sulfate hemihydrate ($CaSO_4{\cdot}0.5H_2O$) can be produced.[25,26] As noted above, in order to recycle ammonia, the Solvay process generates a substantial amount of wastewater and solid waste residues. However, our new process provides a feasible solution to these environmental issues while generating commercially viable products: soda ash, ammonium sulfate, or even high-strength gypsum. The main operational steps are described in detail as follows.

First, thérnadite (Na_2SO_4) or mirabilite ($Na_2SO_4{\cdot}10H_2O$) is fed into the mixer (A) with water. $NaHCO_3$ is then produced via reaction 3 and some is deposited on the wall of the towers (B or C). The input brine washes some of the deposit product off the tower walls. Precarbonation is performed at the bottom of tower B or C via mixing carbon dioxide with ammonia gas. The slurry from the tower bottoms is then sent to a rotary filter (D) for separating bicarbonate from the mother liquor and to prepare for the calcination step at (F). According to reactions 5 and 6, calcination liberates carbon dioxide, ammonia, and water vapor as well as the desired product, light Na_2CO_3 (G).

$$2NaHCO_3 \rightarrow CO_2 + H_2O + Na_2CO_3 \quad (5)$$

$$NH_4HCO_3 \rightarrow CO_2 + H_2O + NH_3 \quad (6)$$

The mother liquor is then pumped into (E) and (H) for evaporative crystallization of Na_2SO_4. During the first evaporation of the liquor, part of the Na_2SO_4 is precipitated and recycled back to the feed stream. The Na_2SO_4 and $(NH_4)_2SO_4$ are both saturated at the invariant point during the second stage of the evaporation (J). Now, antisolvent crystallization is introduced by adding a mixed MEA−MEG solvent to the crystallizer (L). The rest of the Na_2SO_4 is salted out and again sent back to the initial stage. After the separation of Na_2SO_4 solids, the filtrate is sent to an air-cooling evaporator (M) to crystallize $(NH_4)_2SO_4$ at room temperature.

2.4. Thermodynamic Approach. A comprehensive thermodynamic model of the solid−liquid phase equilibria for the Na_2SO_4−$(NH_4)_2SO_4$−MEA−MEG−H_2O system needs to be developed to better understand the antisolvent (MEA−MEG−H_2O) crystallization of Na_2SO_4 from the Na_2SO_4−$(NH_4)_2SO_4$ solution. To establish the thermodynamic model of the solid−liquid phase equilibrium for the system and to be able to accurately calculate the solubility of solid phases under operating conditions, it is necessary to establish the chemical equilibrium, solid−liquid equilibrium, mass balance, and electroneutrality equations for the electrolyte solution. We used the E-NRTL electrolyte solution model to calculate the activity coefficients of ions and the activity of water.

2.4.1. Chemical and Phase Equilibria. With the help of Aspen Plus software, the chemical dissociation formulas for the system containing Na_2SO_4, $(NH_4)_2SO_4$, NH_3, CO_2, MEA, MEG and H_2O are given in Table 2.[27]

In the present system, the main salts to be considered in the solid−liquid equilibria include $Na_2SO_4(s)$, $(NH_4)_2SO_4(s)$, $Na_2SO_4{\cdot}10H_2O(s)$, $Na_2CO_3(s)$, and $NaHCO_3(s)$, whose solubility product constants are determined by the standard Gibbs free energy and related with species molality (mol/kg H_2O) and activity coefficients, as shown below.

$$K_{SP,Na_2SO_4} = (m_{Na^+}\gamma_{Na^+})^2(m_{SO_4^{2-}}\gamma_{SO_4^{2-}}) \quad (7)$$

$$K_{SP,(NH_4)_2SO_4} = (m_{NH_4^+}\gamma_{NH_4^+})^2(m_{SO_4^{2-}}\gamma_{SO_4^{2-}}) \quad (8)$$

$$K_{SP,Na_2SO_4{\cdot}10H_2O} = (m_{Na^+}\gamma_{Na^+})^2(m_{SO_4^{2-}}\gamma_{SO_4^{2-}})a_{H_2O}^{10} \quad (9)$$

Aspen Plus expresses the equilibrium constant using empirical eq 10 containing four parameters: A, B, C, and D, which are determined by regressing the phase equilibrium data. Table 3 lists the parameters of the relevant main salts in this study, which can be found in the Aspen Plus' databank.

https://doi.org/10.1021/acsomega.3c07533
ACS Omega 2024, 9, 1265−1277

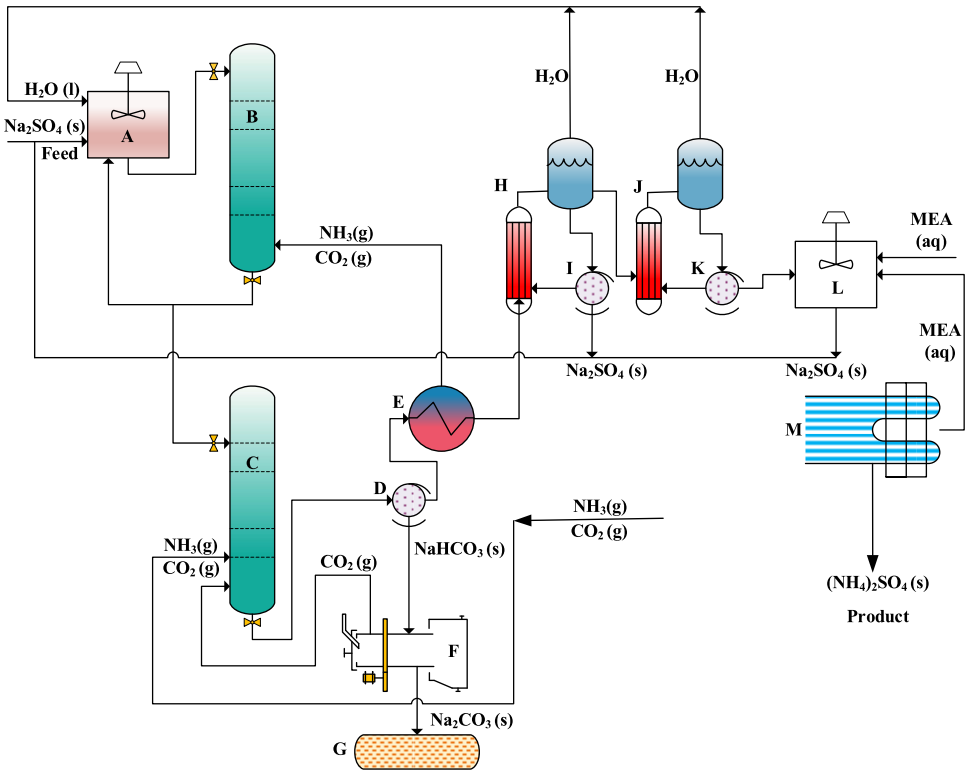

Figure 2. Flow diagram of the new process for manufacturing dense soda based on mixed MEA−MEG antisolvent crystallization: (A) mixer, (B,C) carbonation tower, (D,I,K) filter, (E) heat exchanger, (F) calcination furnace, (G) product tank, (H,J) evaporator, (L) antisolvent crystallization reactor, and (M) air-cooling evaporator.

Table 2. Dissociation Reactions for the $Na^+-NH_4^+-SO_4^{2-}-CO_3^{2-}-NH_3(g)-CO_2(g)-MEA-MEG-H_2O$ System

species	dissociation reaction
H_2O	$2H_2O = H_3O^+ + OH^-$
MEA^{+a}	$MEA^+ + H_2O = MEA + H_3O^+$
$MEACOO^{-b}$	$MEACOO^- + H_2O = MEA + CO_2(aq) + OH^-$
$CO_2(aq)$	$CO_2 + 2H_2O = H_3O^+ + HCO_3^-$
HCO_3^-	$HCO_3^- + H_2O = H_3O^+ + CO_3^{2-}$
HSO_4^-	$HSO_4^- + H_2O = H_3O^+ + SO_4^{2-}$
$NH_3(aq)$	$NH_3(aq) + H_2O = NH_4^- + OH^-$
$(NH_4)_2SO_4(aq)$	$(NH_4)_2SO_4 = 2NH_4^+ + SO_4^-$
$Na_2SO_4(aq)$	$Na_2SO_4 = 2Na^+ + SO_4^{2-}$
$Na_2CO_3(aq)$	$Na_2CO_3 = 2Na^+ + CO_3^{2-}$
$NaHCO_3(s)$	$NaHCO_3(s) = Na^+ + HCO_3^-$
$Na_2CO_3\ H_2O(s)$	$Na_2CO_3\ H_2O(s) = 2Na^+ + CO_3^{2-} + H_2O$
$Na_2CO_3(s)$	$Na_2CO_3(s) = 2Na^+ + CO_3^{2-}$
$Na_2SO_4(s)$	$Na_2SO_4\ (s) = 2Na^+ + SO_4^{2-}$
$Na_2SO_4\ 10H_2O\ (s)$	$Na_2SO_4\ 10H_2O\ (s) = 2Na^+ + SO_4^{2-} + 10H_2O$
$(NH_4)_2SO_4\ (s)$	$(NH_4)_2SO_4\ (s) = 2NH_4^+ + SO_4^-$

[a]$MEAH^+$ is $C_2H_8NO^+$. [b]$MEACOO^-$ is $C_3H_6NO_3^-$.

$$\ln(K_{sp}) = A + B/T + C\ln(T) + DT \tag{10}$$

2.4.2. E-NRTL Equation. The E-NRTL model[27−29] consists of two contributions: a local interaction that exists in the immediate neighborhood of any component and a long-range ionic interaction that exists outside the ion's immediate neighborhood. To account for the long-range ion−ion interactions, the model uses the unsymmetric Pitzer−Debye−Huckel (PDH) expression. For the local interactions, the model uses the local composition concept, as given by the NRTL expression.

$$\ln \gamma_i^{\text{Born}} = \frac{Q_e^2}{2kT}\left(\frac{1}{\varepsilon} - \frac{1}{\varepsilon_w}\right)\frac{z_i^2}{r_i}10^{-2} \tag{11}$$

$$\ln \gamma_i^{\text{PDH}} = -\left(\frac{1000}{M_B}\right)^{1/2} A_\phi \left[\frac{2z_i^2}{\rho}\ln(1+\rho I_x^{1/2}) + \frac{z_i^2 I_x^{1/2} - 2I_x^{1/2}}{1+\rho I_x^{1/2}}\right] S \tag{12}$$

Here, Q_e is the electron charge, ε and ε_w are the dielectric constants of the solvent and water, respectively, r_i is the Born radius. ρ is the "closest approach" parameter of 14.9, A_ϕ, I_x, and M_B are, respectively, the Debye−Huckel parameter, the ionic strength expressed as a mole fraction, and the solvent molecular weight. $\ln\gamma_c^{\text{NRTL}}$, $\ln\gamma_a^{\text{NRTL}}$, and $\ln\gamma_B^{\text{NRTL}}$ are the local composition activity coefficient of cations, anions, and solvents, which can be expressed as

$$\frac{1}{Z_a}\ln \gamma_a^{\text{NRTL}} = \sum_{c'}\left(\frac{X_{c'}}{\sum_{c'} X_{c'}}\right)\frac{\sum_k X_k G_{kc,c,a}\tau_{kc,c,a}}{\sum_k X_k G_{kc,c,a}} + \sum_B \frac{X_B G_{aB}}{\sum_k X_k G_{kB}}\left(\tau_{aB} - \frac{\sum_k X_k G_{kB}\tau_{kB}}{\sum_k X_k G_{kB}}\right) + \sum_c \sum_{a'}\left(\frac{X_{a,}}{\sum_{a''} X_{a''}}\right)\frac{X_c G_{ac,a,c}}{\sum_k X_k G_{kc,a,c}}\left(\tau_{ac,a,c} - \frac{\sum_k X_k G_{kc,a,}\tau_{kc,a,c}}{\sum_k X_k G_{kc,a,c}}\right) \tag{13}$$

https://doi.org/10.1021/acsomega.3c07533
ACS Omega 2024, 9, 1265−1277

Table 3. Coefficients of Equilibrium Constants for Inorganic Salts and Aqueous Species[a]

salts	A	B	C	D
Na_2SO_4	−216.555	4262.38	37.5177	−0.079869
$(NH_4)_2SO_4$	−265.916	−10000	65.896	−0.299478
Na_2SO_4 $10H_2O$	29.9513	−16096.8	1.41556	
Na_2CO_3	−30.468	6566.26		
Na_2CO_3 H_2O	−2270.32	66730.9	387.996	−0.588063
$NaHCO_3$	−63.4345	−1296.96	11.9061	−0.029058
NH_4HCO_3	554.818	−22442.5	−89.0064	0.064732
$MEA^+ + H_2O = MEA + H_3O^+$	−3.03933	−7008.36	0	−0.003135

[a]The concentration basis for equilibrium constants K_{eq} is the mole fraction (default) and T is the temperature in °C.

$$\ln \gamma_B^{NRTL} = \frac{\sum_j X_j G_{jB}\tau_{jB}}{\sum_k X_k G_{kB}} + \sum_{B'} \frac{X_{B,} G_{BB,}}{\sum_k X_k G_{kB,}} \left(\tau_{BB,} - \frac{\sum_k X_k G_{kB,}\tau_{kB,}}{\sum_k X_k G_{kB,}}\right) + \sum_c \sum_{a'} \left(\frac{X_{a,}}{\sum_{a''} X_{a''}}\right) \frac{X_c G_{Bc,a,c}}{\sum_k X_k G_{kc,a,c}} \left(\tau_{ac,a,c} - \frac{\sum_k X_k G_{kc,a,}\tau_{kc,a,c}}{\sum_k X_k G_{kc,a,c}}\right) + \sum_a \sum_{c'} \left(\frac{X_{c,}}{\sum_{c''} X_{c''}}\right) \frac{X_a G_{Ba,c,a}}{\sum_k X_k G_{ka,c,a}} \left(\tau_{Bc,c,a} - \frac{\sum_k X_k G_{ka,c,}\tau_{ka,c,a}}{\sum_k X_k G_{ka,c,a}}\right) \quad (14)$$

with $\ln G_{ka,c'a} = -\tau_{ka,c'a}\alpha$, $\tau_{cB} = \tau_{aB} = \tau_{ca,B}$; $\tau_{Bc} = \tau_{Ba} = \tau_{B,ca}$; $\tau_{Bc,ac} = \tau_{Ba,ca} = \tau_{B,ca}$

$$\tau_{ca,w} = C_{ca,w} + \frac{D_{ca,w}}{T} + E_{ca,w}\left[\frac{(T^\circ - T)}{T} + \ln\left(\frac{T}{T^\circ}\right)\right] \quad (15)$$

$$\tau_{w,ca} = C_{w,ca} + \frac{D_{w,ca}}{T} + E_{W,ca}\left[\frac{(T^\circ - T)}{T} + \ln\left(\frac{T}{T^\circ}\right)\right] \quad (16)$$

where X_j is the effective molar fraction of component j, which can be calculated from x_jZ_j; τ is the energy parameter and α is a nonrandom factor; T° is the reference temperature of 298.15 K; subscripts w and ca denote the solvent (water) and electrolyte (cation−anion), respectively. Usually, the value of α is equal to 0.3 for molecule−molecule interactions and 0.2 for electrolyte−molecule interactions. C, D, and E are empirical parameters that can be obtained by regressing the experimental data.

The solid−liquid equilibrium data for the Na_2SO_4−$(NH_4)_2SO_4$−MEA−MEG−H_2O system has not yet been fully reported so the Aspen Plus database lacks the necessary model parameters. Our laboratory had to determine the solid−liquid equilibrium data, or solubility data while using Aspen Plus to regress the E-NRTL model parameters for the activity coefficients. The obtained model parameters can be directly added to Aspen Plus' database for future simulation calculations of crystallization processes.

2.5. Solubility Measurements. The solubility of readily soluble inorganic salts can be determined by the dynamic dissolution method because high solubilities imply that more salts are dissolved per unit solvent weight, and thus, the relative error in the measured solubility is minimized. The equilibrium precipitation method, on the other hand, introduces a large error, because it requires a large amount of solvent and a long equilibration time. It also requires determination of the nature of the solid phase precipitate and the composition of the liquid phase via chemical analysis, both of which also introduce further measurement errors. Hence, we decided to use the dissolution method to measure the solubility of Na_2SO_4 and $(NH_4)_2SO_4$ in aqueous MEG and mixed MEA−MEG solutions at different temperatures and various concentration levels. The detailed procedure for the solubility experiments has been described previously,[15] so only a brief summary will be given here. After the weighed solution was added to a 100 mL jacketed glass bottle with magnetic stirring, the temperature inside the reactor was accurately measured by a thermometer, and the temperature was controlled by recirculating water from a water bath to ±0.1 K. An electronic balance (AL104; Mettler-Toledo) with a precision of 0.001 g was used. Once the specified temperature was reached, salt was gradually added to the solution. We usually waited more than 5 h for crystal dissolution until only a very small number of particles floated in the reactor. At this point, the total mass of the salt added to the solution represents the solubility.

2.6. Antisolvent Crystallization. A semibatch antisolvent crystallization reactor, shown in Figure 3, was used to test the effects of the crystallization using the MEA−MEG cosolvent. The saturated aqueous solution of Na_2SO_4 and $(NH_4)_2SO_4$ was first charged into a 1.5 L reactor.

The temperature was initially set at 353 K with an agitation speed of 400 rpm. While stirring the reactor solution, a peristaltic pump was used to pump the MEA−MEG solution into the reactor until it reached 50 wt % (salt-free) MEA−MEG. Through this MEA−MEG addition, Na_2SO_4's solubility dramatically decreases, and antisolvent crystallization proceeds. Under these operating conditions, most of the Na_2SO_4 precipitated out. We filtered the Na_2SO_4 crystals for characterization with XRD and SEM and reused the filtrate that mostly contained $(NH_4)_2SO_4$ and a small portion of sodium sulfate. The temperature was then adjusted from 353 to 293 K for the cooling evaporative crystallization of ammonium sulfate. Following the evaporative crystallization, solid−liquid separation yielded a filtrate containing MEA−MEG and a certain amount of soluble $(NH_4)_2SO_4$, which was recycled for the next feed as an antisolvent. The crystallized $(NH_4)_2SO_4$ was characterized by XRD and SEM.

3. RESULTS AND DISCUSSION

3.1. Solubility Measurements. We recently reported and modeled the phase equilibria for the system Na_2SO_4−

https://doi.org/10.1021/acsomega.3c07533
ACS Omega 2024, 9, 1265−1277

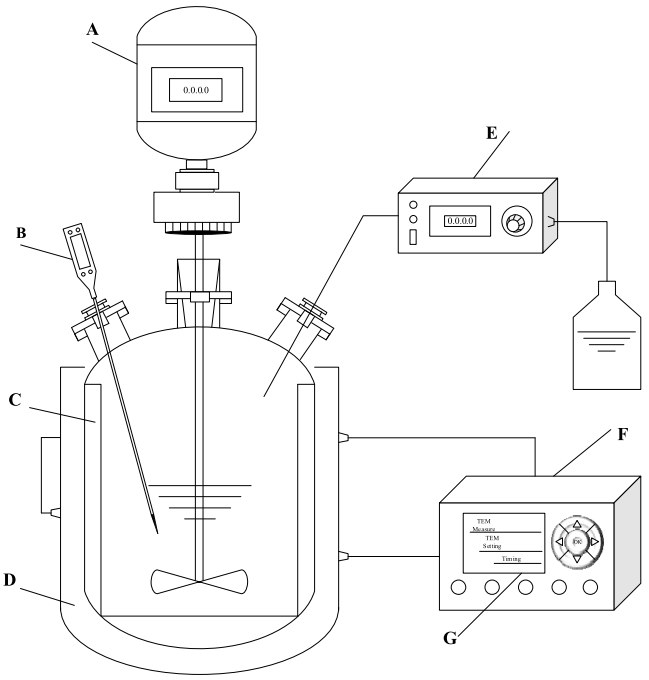

Figure 3. Schematic diagram for the antisolvent crystallization reactor used to separate Na_2SO_4 from $(NH_4)_2SO_4$ aqueous solution using MEA−MEG solvent mixtures: (A) agitator, (B) thermometer, (C) baffle, (D) water bath, (E) peristaltic pump, (F) temperature controller, and (G) bath thermometer.

$(NH_4)_2SO_4$−MEA−H_2O.[15] The solubility of sodium sulfate across the entire range of MEG concentration was investigated at temperatures from 25 to 100 °C and it sharply decreased with increasing MEG concentration due to the salting-out effect.[30] Comparing the magnitude of the solubility of Na_2SO_4 in MEG or MEA, it is clear that the decrease in solubility is more marked in MEA, indicating a greater salting-out effect. However, the solubilities of Na_2SO_4 and $(NH_4)_2SO_4$ in MEG or mixed MEG−MEA solutions were not available in the literature.

3.1.1. Solubility of $(NH_4)_2SO_4$ (s) in the System: MEG−H_2O. The solubility of $(NH_4)_2SO_4$ was measured from 293 to 353 K at varying concentrations (x) of MEG (Table 4 and Figure 4). The solubility of $(NH_4)_2SO_4$ increases with increasing temperature but decreases with the addition of MEG up to an MEG mole fraction of 0.3. However, the solubility of $(NH_4)_2SO_4$ in MEA[15] increases with the concentration of this solvent. For a mixed MEA−MEG antisolvent crystallization process, we wanted the solubility of Na_2SO_4 and $(NH_4)_2SO_4$ to be sufficiently different to achieve maximum crystallization yields of one over the other. Thus, based on Figure 4, the amount of MEG in the solvent mixture needs to be low enough to retain high $(NH_4)_2SO_4$ solubility.

3.1.2. Solubility of Na_2SO_4(s) in the System $(NH_4)_2SO_4$−MEG−H_2O. The effect of $(NH_4)_2SO_4$ concentration in the MEG aqueous solution on the solubility of Na_2SO_4 was investigated from 293 to 353 K at increments of 10 K, as shown in Figure 5 and Table 5. This set of experiments was organized in such a way that an aqueous solution of the full concentration range of MEG was first prepared, and then, $(NH_4)_2SO_4$ solid was added to the solution at 293.15 K until saturation. From there, the temperature was increased, and the solubility of Na_2SO_4 in this solution was determined. The initial solutions contained MEG in concentrations ranging from 5 to 86 wt % and $(NH_4)_2SO_4$ from 2.9 to 34 wt %. However, it can be seen from Figure 6 that the solubility of Na_2SO_4 in the solution first increases with increasing MEG concentration and then decreases beyond 40 wt % MEG.

Table 4. Experimental Solubility of $(NH_4)_2SO_4$(s)(1) in the MEG(2)-H_2O(3) System at 101.3 kPa[a]

$100w_1$ (wt %)	$100w_2$ (wt %)	$100w_3$ (wt %)	x_1	x_2	x_3
T = 293.15 K					
1.51	98.49	0.00	0.0071	0.9929	0.0000
2.95	87.23	9.82	0.0113	0.7124	0.2762
4.90	76.36	18.75	0.0161	0.5330	0.4509
8.33	64.10	27.56	0.0240	0.3933	0.5827
12.15	52.65	35.20	0.0318	0.2931	0.6752
16.73	41.33	41.94	0.0406	0.2134	0.7460
22.62	30.89	46.49	0.0527	0.1532	0.7942
28.50	21.38	50.11	0.0645	0.1031	0.8324
33.88	13.33	52.79	0.0754	0.0631	0.8615
37.76	6.30	55.94	0.0818	0.0291	0.8891
42.94	0.00	57.06	0.0931	0.0000	0.9069
T = 313.15 K					
2.05	97.95	0.00	0.0097	0.9903	0.0000
3.68	86.57	9.74	0.0142	0.7104	0.2754
6.00	75.47	18.53	0.0198	0.5310	0.4492
9.12	63.55	27.33	0.0264	0.3923	0.5812
13.04	52.12	34.85	0.0343	0.2923	0.6734
18.24	40.58	41.18	0.0448	0.2124	0.7427
24.18	30.27	45.55	0.0572	0.1524	0.7904
30.16	20.89	48.95	0.0696	0.1025	0.8279
35.69	12.96	51.35	0.0811	0.0627	0.8561
40.17	6.05	53.78	0.0898	0.0288	0.8814
44.61	0.00	55.39	0.0989	0.0000	0.9011
T = 333.15 K					
2.05	97.95	0.00	0.0097	0.9903	0.0000
4.40	85.93	9.67	0.0170	0.7083	0.2746
6.96	74.70	18.34	0.0232	0.5292	0.4476
9.89	63.02	27.10	0.0288	0.3914	0.5798
14.39	51.31	34.31	0.0383	0.2911	0.6706
19.97	39.72	40.31	0.0499	0.2113	0.7388
26.10	29.50	44.40	0.0630	0.1515	0.7855
32.42	20.21	47.37	0.0767	0.1017	0.8216
37.67	12.56	49.77	0.0877	0.0623	0.8500
41.92	5.88	52.20	0.0958	0.0286	0.8755
46.57	0.00	53.43	0.1062	0.0000	0.8938
T = 353.15 K					
2.05	97.95	0.00	0.0097	0.9903	0.0000
5.11	85.29	9.60	0.0199	0.7063	0.2739
7.91	73.94	18.15	0.0265	0.5274	0.4461
10.91	62.30	26.79	0.0321	0.3901	0.5779
15.28	50.77	33.95	0.0410	0.2903	0.6687
21.43	39.00	39.57	0.0543	0.2103	0.7354
27.61	28.90	43.49	0.0676	0.1508	0.7816
33.55	19.87	46.58	0.0804	0.1013	0.8183
39.21	12.25	48.54	0.0931	0.0619	0.8450
43.40	5.73	50.88	0.1012	0.0284	0.8704
48.39	0.00	51.61	0.1133	0.0000	0.8867

[a]Standard uncertainties are $u(T)$ = 0.01 K, $u(P)$ = 0.4 kPa, $u(x)$ = 0.02, and u(wt %) = 0.02; equilibrium temperature (T), liquid mole fraction (x), liquid mass percentage (wt %).

3.1.3. Solubility of Na_2SO_4(s) or $(NH_4)_2SO_4$(s) in the System MEA−MEG−H_2O. The solubility of Na_2SO_4 and $(NH_4)_2SO_4$ in a mixed MEA−MEG aqueous solution was also determined from 298 to 353 K as shown in Table 6 and Figure 6 for Na_2SO_4

https://doi.org/10.1021/acsomega.3c07533
ACS Omega 2024, 9, 1265−1277

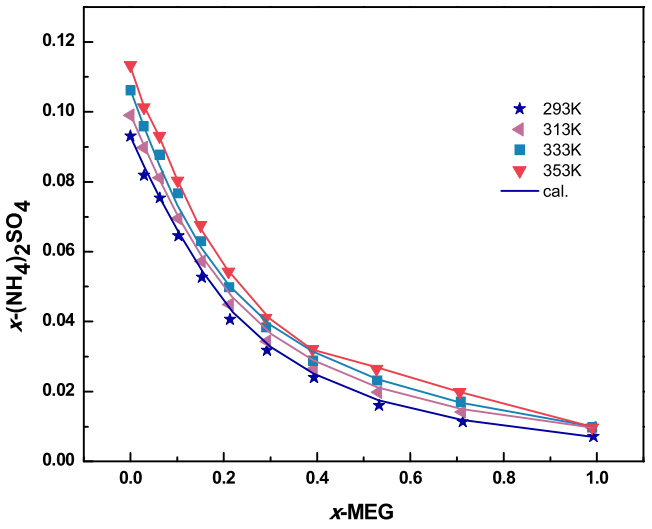

Figure 4. Solubility of $(NH_4)_2SO_4$ solids in aqueous MEG solutions at 293, 313, 333, and 353 K; p = 0.1 MPa; dots: experimental data; solid lines: model calculation using newly obtained parameters.

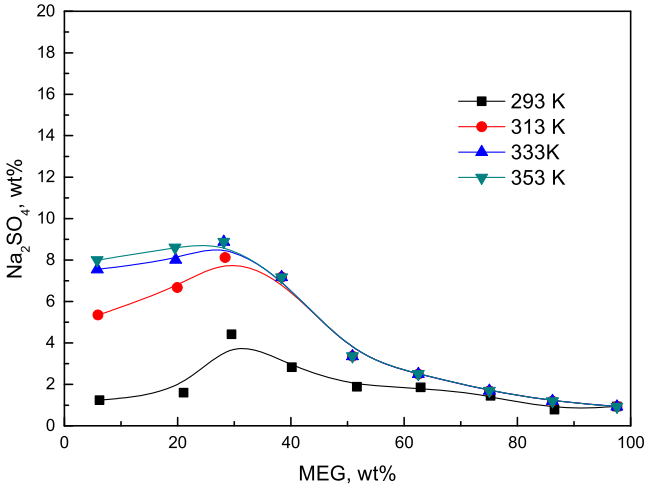

Figure 5. Solubility of $Na_2SO_4(4)(s)$ in the $H_2O(1)$−MEG(2)−$(NH_4)_2SO_4(3)$ system.

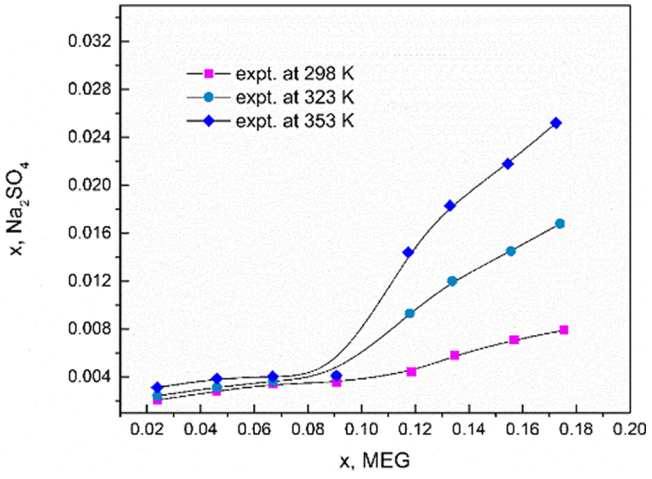

Figure 6. Solubility of $Na_2SO_4(s)$ in the mixed MEA−MEG solution at the ratio of (MEA+MGA):H_2O = 50:50 (w/w).

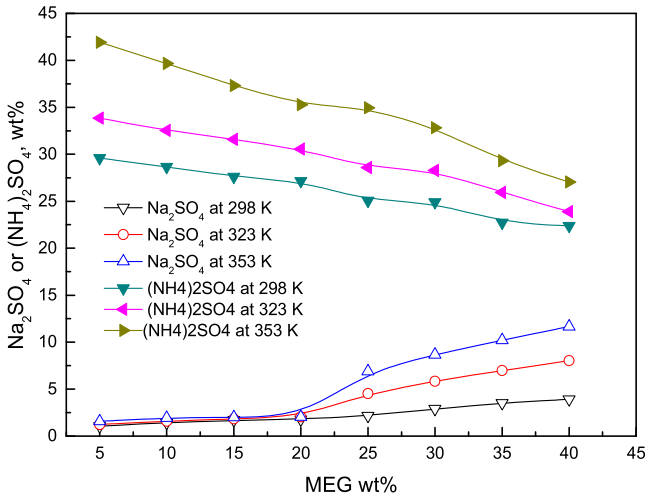

Figure 7. Comparison of the solubility of $Na_2SO_4(s)$ or $(NH_4)_2SO_4(s)$ in the mixed MEA−MEG solution at a (MEA+MGA):H2O ratio of 50:50.

and in Table 7 and Figure 7 for $(NH_4)_2SO_4$. The ratio of the sum of the weights of the two solvents MEA and MEG to the weight of water was kept fixed at 1:1, but the ratio of the weights of MEA and MEG was varied. Figure 6 shows that, up to a mole fraction of MEG of 0.09, the solubility of Na_2SO_4 does not change significantly with both the temperature and MEG concentration. However, as the concentration of MEG is increased, these two factors have a significant effect on the solubility of Na_2SO_4, which increases rapidly. In the antisolvent crystallization separation of Na_2SO_4 and $(NH_4)_2SO_4$, the ideal situation is that the solubility of Na_2SO_4 in the mixed solvent is as low as possible, even at higher temperatures. As can be seen from Figure 6, this ideal situation requires that the mole fraction of the solvent MEG not exceed 0.09.

The solubility of $(NH_4)_2SO_4$ increases significantly with temperature but decreases slowly with increasing MEG concentration (Figure 7). It should be noted that the value of the x coordinate in Figure 7 is the initial concentration of MEG to make it easier for the reader to understand the effect of the concentration of the starting solvent mixture on the solubility of the two inorganic salts. Figure 7 also shows that the initial concentration of 20−25 wt % MEG, although higher than the ideal situation described above, still effectively achieves the separation of Na_2SO_4 and $(NH_4)_2SO_4$. Further, higher concentrations of MEG in the mixed solvent serve to limit the degradation of the MEA components at higher temperatures.

3.2. Thermodynamic Modeling. In order to model the salt separation process, we needed to build a consistent and comprehensive thermodynamic model for the Aspen Plus platform. The model can be used to simulate the proposed process, enabling subsequent engineering and process design. To build the model, we used the experimentally obtained solubility data to evaluate the default parameters in Aspen Plus. Due to the absence of the main E-NRTL model parameters, Aspen Plus gave calculation results with such a large error that the experimental data had to be used to regress the necessary model parameters to improve the accuracy of the solid−liquid equilibrium calculations.

For the phase equilibrium of the $Na_2SO_4(s)$−$(NH_4)_2SO_4$−H_2O system,[15] there are two cations (Na^+ and NH_4^+) and two anions (SO_4^{2-} and HSO_4^-). The binary interaction parameters for the 4 water−electrolyte pairs: (Na^+ SO_4^{2-}):H_2O, (Na^+

https://doi.org/10.1021/acsomega.3c07533
ACS Omega 2024, 9, 1265−1277

Table 5. Experimental Solubility of Na_2SO_4(4)(s) in the H_2O(1)−MEG(2)−$(NH_4)_2SO_4$(3) System at 101.3 kPa[a]

$100w_1$ (wt %)	$100w_2$ (wt %)	$100w_3$ (wt %)	$100w_4$ (wt %)	x_1	x_2	x_3	x_4
			T = 293.15 K				
9.73	86.56	2.93	0.78	0.2751	0.7094	0.0112	0.0043
18.46	75.26	4.83	1.45	0.4485	0.5303	0.0159	0.0052
27.04	62.93	8.18	1.86	0.5787	0.3906	0.0238	0.0068
34.52	51.66	11.92	1.89	0.6695	0.2906	0.0315	0.0084
40.73	40.17	16.27	2.83	0.7333	0.2097	0.0398	0.0171
44.41	29.54	21.63	4.42	0.7792	0.1503	0.0516	0.0188
49.29	21.05	28.06	1.60	0.8200	0.1015	0.0635	0.0148
55.23	6.22	37.31	1.24	0.8791	0.0287	0.0809	0.0113
			T = 313.15 K				
9.69	86.20	2.92	1.19	0.2751	0.7094	0.0113	0.0042
18.42	75.07	4.82	1.69	0.4485	0.5303	0.0160	0.0052
26.86	62.51	8.13	2.50	0.5787	0.3906	0.0239	0.0068
34.00	50.89	11.75	3.36	0.6695	0.2906	0.0315	0.0083
38.91	38.38	15.54	7.17	0.7333	0.2097	0.0399	0.0171
42.69	28.39	20.79	8.12	0.7792	0.1503	0.0517	0.0187
46.75	19.96	26.61	6.67	0.8200	0.1015	0.0636	0.0148
52.93	5.96	35.76	5.35	0.8791	0.0287	0.0809	0.0112
			T = 333.15 K				
9.69	86.198	2.92	1.19	0.2751	0.7094	0.0113	0.0043
18.42	75.074	4.82	1.69	0.4485	0.5303	0.0160	0.0052
26.86	62.512	8.13	2.50	0.5787	0.3906	0.0239	0.0068
34.00	50.891	11.75	3.36	0.6695	0.2906	0.0315	0.0084
38.91	38.379	15.54	7.17	0.7333	0.2097	0.0399	0.0171
42.34	28.159	20.62	8.88	0.7777	0.1500	0.0516	0.0207
46.08	19.677	26.23	8.01	0.8174	0.1012	0.0634	0.0180
51.70	5.825	34.93	7.55	0.8747	0.0286	0.0805	0.0162
			T = 353.15 K				
9.69	86.20	2.92	1.190	0.2751	0.7094	0.0113	0.0043
18.42	75.07	4.82	1.693	0.4485	0.5303	0.0160	0.0052
26.86	62.51	8.13	2.503	0.5787	0.3906	0.0239	0.0068
34.00	50.89	11.75	3.363	0.6695	0.2906	0.0315	0.0084
38.91	38.38	15.54	7.167	0.7333	0.2097	0.0399	0.0171
42.34	28.16	20.62	8.882	0.7777	0.1500	0.0516	0.0207
45.78	19.55	26.06	8.609	0.8162	0.1011	0.0633	0.0195
51.45	5.80	34.76	7.992	0.8738	0.0286	0.0804	0.0172

[a]Standard uncertainties are $u(T)$ = 0.01 K, $u(P)$ = 0.4 kPa, $u(x)$ = 0.02, and u(wt %) = 0.02; equilibrium temperature (T), liquid mole fraction (x), liquid mass percentage (wt %).

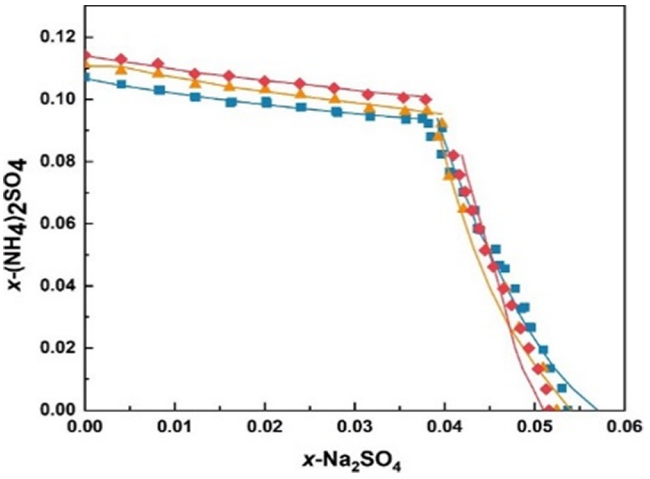

Figure 8. Solubility phase diagram of Na_2SO_4 and $(NH_4)_2SO_4$ in aqueous solutions at 333, 343, and 353 K; p = 0.1 MPa; dots: experimental data; solid lines: Aspen calculations were performed using newly obtained model parameters.

HSO_4^-):H_2O, (NH_4^+ SO_4^{2-}):H_2O and (NH_4^+ HSO_4^-):H_2O; and the 6 electrolyte-electrolyte pairs: (Na^+ SO_4^{2-}):(NH_4^+ SO_4^{2-}), (Na^+ SO_4^{2-}):(Na^+ HSO_4^-), (NH_4^+ SO_4^{2-}):(Na^+ HSO_4^-), (NH_4^+ SO_4^{2-}):(NH_4^+ HSO_4^-), (Na^+ HSO_4^-):(NH_4^+ HSO_4^-), and (Na^+ SO_4^{2-}):(NH_4^+ HSO_4^-), are required to fully characterize the system. Yan and Chen[29] reported the parameters for the (Na^+ SO_4^{2-}):H_2O pair and the parameters for the (NH_4^+ SO_4^{2-}):H_2O pair are available in Aspen Properties[28] version 8.8. The phase equilibrium data of the Na_2SO_4(s)−$(NH_4)_2SO_4$−H_2O reported by Li et al.[15] were regressed to obtain the binary interaction parameters (C, D, and E) for the (Na^+ SO_4^{2-}):(NH_4^+ SO_4^{2-}) pair, which are given in Table 8. The modeling results for the system are shown in Figure 8 in which the calculated solid liquid equilibria are compared to experimental data, indicating very good agreement.

With the binary interaction parameters for the aqueous Na_2SO_4−$(NH_4)_2SO_4$ system, we used the E-NRTL activity coefficient model embedded in Aspen Plus to model the system Na_2SO_4−MEA−H_2O using the experimental solubility[15] of solid Na_2SO_4 in aqueous MEA solution at 353 K. The regressed solubility using the newly obtained E-NRTL parameters for the

https://doi.org/10.1021/acsomega.3c07533
ACS Omega 2024, 9, 1265−1277

Table 6. Experimental Solubility for the Na_2SO_4(s)(1)−MEA(2)−MEG(3)−H_2O(4) System at 101.3 kPa[a]

100w$_1$ (wt %)	100w$_2$ (wt %)	100w$_3$ (wt %)	100w$_4$ (wt %)	x_1	x_2	x_3	x_4
T = 298.15 K, solids: Na_2SO_4							
(MEA+MGA):H_2O = 50:50, varied MEA and varied MEG)							
1.05	44.02	5.31	49.62	0.00207	0.2018	0.0239	0.7721
1.42	38.85	10.20	49.52	0.00281	0.1785	0.0461	0.7724
1.72	34.48	14.73	49.07	0.00342	0.1594	0.0670	0.7700
1.76	29.38	19.90	48.95	0.00352	0.1361	0.0907	0.7696
2.17	24.02	25.72	48.09	0.0044	0.1125	0.1186	0.7645
2.90	19.34	29.28	48.49	0.0058	0.0904	0.1347	0.7691
3.52	14.22	33.96	48.30	0.0071	0.0667	0.1569	0.7693
3.92	9.84	37.95	48.29	0.0079	0.0462	0.1755	0.7703
T = 323.15 K, solids: Na_2SO_4							
(MEA+MGA):H_2O = 50:50, varied MEA and varied MEG)							
1.23	43.94	5.30	49.53	0.00242	0.2017	0.0239	0.7718
1.59	38.79	10.19	49.44	0.00315	0.1785	0.0461	0.7722
1.83	34.45	14.71	49.01	0.00364	0.1594	0.0670	0.7699
2.06	29.30	19.84	48.81	0.00410	0.1360	0.0906	0.7692
4.53	23.44	25.10	46.93	0.0093	0.1120	0.1180	0.7607
5.84	18.75	28.39	47.02	0.0120	0.0898	0.1338	0.7643
6.99	13.71	32.74	46.57	0.0145	0.0662	0.1557	0.7636
8.03	9.42	36.33	46.23	0.0168	0.0458	0.1740	0.7634
T = 353.15 K, solids: Na_2SO_4							
(MEA+MGA):H_2O = 50:50, varied MEA and varied MEG)							
1.58	43.79	5.28	49.35	0.00313	0.20163	0.0239	0.7712
1.94	38.65	10.15	49.26	0.00387	0.17839	0.0461	0.7716
2.02	34.38	14.68	48.92	0.00404	0.15937	0.0669	0.7695
2.05	29.30	19.84	48.81	0.00410	0.13604	0.0906	0.7691
6.89	22.86	24.48	45.77	0.0144	0.1114	0.1174	0.7568
8.67	18.19	27.54	45.61	0.0183	0.0892	0.1330	0.7595
10.21	13.23	31.61	44.95	0.0218	0.0657	0.1545	0.7579
11.66	9.05	34.89	44.40	0.0252	0.0454	0.1725	0.7569

[a]Standard uncertainties are $u(T)$ = 0.01 K, $u(P)$ = 0.4 kPa, $u(x)$ = 0.02, and u(wt %) = 0.02; equilibrium temperature (T), liquid mole fraction (x), liquid mass percentage (wt %).

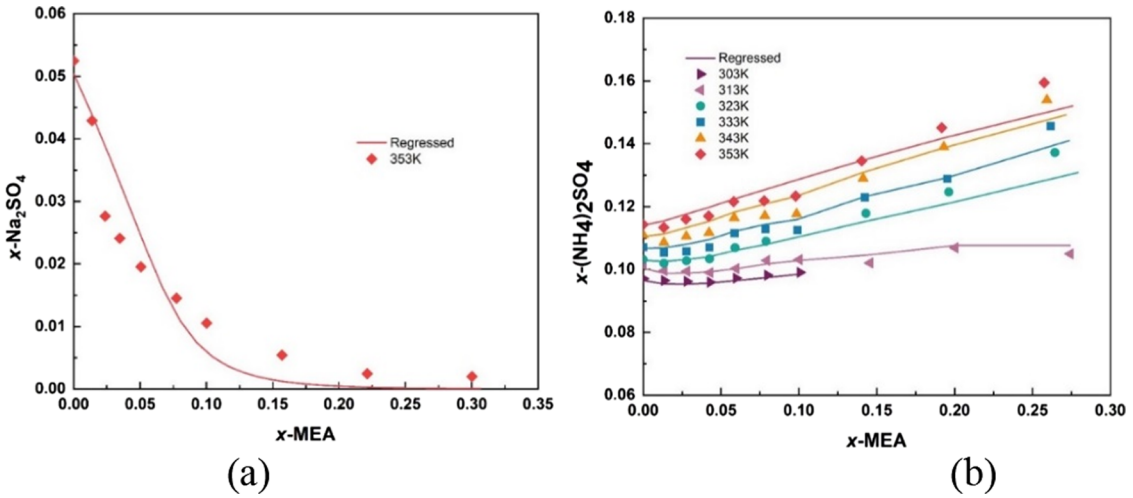

Figure 9. (a) Solubility of Na_2SO_4 in aqueous MEA solutions at 353 K; p = 0.1 MPa; dots: experimental data; solid lines: Aspen calculations were performed using newly obtained parameters. (b) Solubility of $(NH_4)_2SO_4$ in aqueous MEA solutions at 303−353 K; p = 0.1 MPa; dots: experimental data; solid lines: Aspen calculation using newly obtained parameters.

(Na^+ SO_4^{2-}):MEA pair is compared with the experimental data in Figure 9a with good results (average mole fraction deviation is less than 0.015). Similarly, good results were obtained by modeling the solubility of $(NH_4)_2SO_4$ in an aqueous MEA solution, as shown in Figure 9b. The new E-NRTL interaction parameters for the (NH_4^+ SO_4^{2-}):MEA pair are given in Table 8.

In previous work,[15] the mixed solvent electrolyte (MSE) model developed by OLI Systems was successfully applied to regress the phase of the systems: Na_2SO_4(s)−$(NH_4)_2SO_4$−H_2O and $(NH_4)SO_4$−MEA−H_2O. However, for Na_2SO_4(s)−MEA−H_2O, MSE parameter regression resulted in large deviations. Fortunately, OLI gave reasonable predictions using its own

https://doi.org/10.1021/acsomega.3c07533
ACS Omega 2024, 9, 1265−1277

Table 7. Experimental Solubility of $(NH_4)_2SO_4(s)(1)$ in the MEA(2)−MEG(3)-H_2O(4) System at 101.3 kPa[a]

100w$_1$ (wt%)	100w$_2$ (wt%)	100w$_3$ (wt%)	100w$_4$ (wt%)	x_1	x_2	x_3	x_4
T = 298.15 K, solids: $(NH_4)_2SO_4$							
l MEA and varied MEG)							
29.59	31.70	3.77	34.94	0.0816	0.1890	0.0221	0.7072
28.66	28.61	7.47	35.26	0.0784	0.1694	0.0435	0.7086
27.61	25.44	10.92	36.02	0.0745	0.1486	0.0627	0.7140
27.15	21.58	15.09	36.18	0.0730	0.1256	0.0864	0.7148
25.05	18.66	19.03	37.27	0.0660	0.1063	0.1067	0.7209
24.90	14.66	22.77	37.67	0.0652	0.0831	0.1270	0.7246
22.72	11.43	27.53	38.33	0.0586	0.0638	0.1513	0.7263
22.38	7.96	31.20	38.45	0.0576	0.0444	0.1711	0.7269
T = 323.15 K, solids: $(NH_4)_2SO_4$							
d MEA and varied MEG							
33.85	29.78	3.54	32.82	0.0976	0.1857	0.0217	0.6948
32.54	27.05	7.06	33.34	0.0927	0.1667	0.0428	0.6976
31.59	24.05	10.32	34.04	0.0888	0.1463	0.0618	0.7030
30.55	20.57	14.38	34.49	0.0851	0.1240	0.0853	0.7055
28.58	17.78	18.13	35.51	0.0780	0.1050	0.1054	0.7117
28.28	14.00	21.75	35.97	0.0766	0.0821	0.1255	0.7158
25.94	10.95	26.38	36.73	0.0691	0.0631	0.1496	0.7182
23.90	7.81	30.59	37.70	0.0625	0.0441	0.1702	0.7232
T = 353.15 K, solids: $(NH_4)_2SO_4$							
l MEA and varied MEG)							
41.92	26.15	3.11	28.82	0.1323	0.1786	0.0209	0.6680
39.66	24.20	6.32	29.82	0.1222	0.1613	0.0414	0.6749
37.31	22.03	9.46	31.19	0.1116	0.1426	0.0602	0.6853
35.28	19.17	13.41	32.14	0.1034	0.1215	0.0836	0.6914
34.94	16.19	16.51	32.35	0.1020	0.1022	0.1026	0.6931
32.82	13.11	20.37	33.70	0.0932	0.0806	0.1232	0.7029
29.32	10.45	25.18	35.06	0.0808	0.0623	0.1477	0.7092
27.06	7.48	29.32	36.14	0.0729	0.0436	0.1683	0.7151

[a]Standard uncertainties are $u(T)$ = 0.01 K, $u(P)$ = 0.4 kPa, $u(x)$ = 0.02, and u(wt%) = 0.02; equilibrium temperature (T), liquid mole fraction (x), liquid mass percentage (wt%).

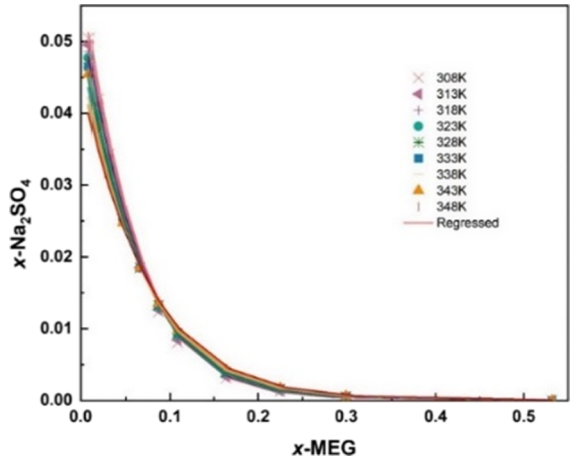

Figure 10. Solubility of Na_2SO_4 in aqueous MEG solutions at 353 K; p = 0.1 MPa; dots: experimental data; solid lines: Aspen calculation using newly obtained parameters.

parameters. The above results show that the E-NRTL model gives accurate calculations for this system, which provides a good basis for future process simulation.

Having regressed the interaction parameters for the system $Na_2SO_4(s)$−$(NH_4)_2SO_4$−MEA−H_2O with confidence, we expand the methodology to the cosolvent system $Na_2SO_4(s)$−$(NH_4)_2SO_4$−MEG−H_2O. Figure 10 shows that the E-NRLT model successfully represents the solubility of Na_2SO_4 in aqueous MEG solution with the help of regressed literature data.[30] Similar modeling results were obtained for the $(NH_4)_2SO_4$−MEG−H_2O system as shown in Figure 4. The newly obtained model parameters for the (Na^+ SO_4^{2-}):MEG pair, the (Na^+ HSO_4^-):MEG pair, (NH_4^+ SO_4^{2-}):MEG pair and (NH_4^+ HSO_4^-):MEG pair are also tabulated in Table 8.

Having fully identified the binary interaction parameters for modeling the solubility of Na_2SO_4 and $(NH_4)_2SO_4$ in the MEA−H_2O and MEG−H_2O systems, we now can use the model to predict the solubility of both salts in the mixed MEA−MEG solvent aqueous solution. The prediction accuracy was evaluated by using the experimental data listed in Tables 6 and 7, and the total average mole fraction deviation is less than 0.02(x).

3.3. Antisolvent Crystallization and Validation of the New Process. With the thermodynamic model for the Na_2SO_4−$(NH_4)_2SO_4$−MEA−MEG aqueous solution, we tested the ability of the antisolvent crystallization routes for the separation of both salts. Initially, the crystallizer was loaded with 500 mL of aqueous solution of Na_2SO_4 and $(NH_4)_2SO_4$ at the concentrations of 2.5 and 6.5 mol/kg H_2O (the invariant point); i.e., both solids were saturated in solution. The temperature was kept constant throughout the run at 353 K. The mixed MEA and MGE solvent at a 50:50 weight ratio was then added to the solution using a calibrated peristaltic pump until a 50:50 ratio of solvent to water was reached. The precipitation of Na_2SO_4 crystals was observed as solvent was

https://doi.org/10.1021/acsomega.3c07533
ACS Omega 2024, 9, 1265−1277

Table 8. E-NRTL Parameters of Interaction between Species in the System Na_2SO_4−$(NH_4)_2SO_4$−MEA−MEG−H_2O

parameter no.	molecule i or ion i		molecule j or ion j		C	D	E	α
1	H_2O		H_3O^+	HSO_4^-	6.362	1958.2	−4.599	0.2
	H_3O^+	HSO_4^-	H_2O		−3.749	−583.2	4.472	0.2
2	H_2O		H_3O^+	OH^-	8.045			
	H_3O^+	OH^-	H_2O		−4.072			
3	H_2O		H_3O^+	SO_4^-	8	0		
	H_3O^+	SO_4^-	H_2O		−4	0		
4	H_2O		NH_4^+	HSO_4^-	7.665	−10000		
	NH_4^+	HSO_4^-	H_2O		−3.884	−10000		
5	H_2O		NH_4^+	OH^-	8.045			
	NH_4^+	OH^-	H_2O		−4.072			
6	H_2O		NH_4^+	SO_4^-	7.628			
	NH_4^+	SO_4^-	H_2O		−3.701			
7	H_2O		Na^+	HSO_4^-	7.663			
	Na^+	HSO_4^-	H_2O		−3.944			
8	H_2O		Na^+	OH^-	6.738	1420.24	3.01393	
	Na^+	OH^-	H_2O		−3.77122	−471.82	2.13656	
9	H_2O		Na^+	SO_4^-	1.9545	1762.19	7.55242	0.2
	Na^+	SO_4^-	H_2O		−2.03326	−537.968	0.00691975	0.2
10	MEA		MEA^+	OH^-	15	0	0	0.1
	MEA^+	OH^-	MEA		−8	0	0	0.1
11	MEA		H_3O^+	OH^-	15	0	0	0.1
	H_3O^+	OH^-	MEA		−8	0	0	0.1
12	$H_2SO_4^-$		H_3O^+	HSO_4^-	12.992	−1732.9	−30.126	0.2
	H_3O^+	HSO_4^-	$H_2SO_4^-$		−2.981	−162.3	0.806	0.2
13	$H_2SO_4^-$		H_3O^+	SO_4^-	8	0		
	H_3O^+	SO_4^-	$H_2SO_4^-$		−4	0		
14	Na^+	OH^-	Na^+	SO_4^-	0	0	0	
	Na^+	SO_4^-	Na^+	OH^-	0	0	0	
15[a]	Na^+	SO_4^-	NH_4^+	SO_4^-	**32.1634**	**−10000**	**−250.057**	
	NH_4^+	SO_4^-	Na^+	SO_4^-	**22.0603**	**−7050.36**	**−147.857**	
16[a]	MEA		Na^+	SO_4^-	**1.93795**	**−0.79162**		
	Na^+	SO_4^-	MEA		**7.21825**	**−16.7209**		
17[a]	MEA		NH_4^+	SO_4^-	**−2.95214**	**716.658**		
	NH_4^+	SO_4^-	MEA		**−16.5523**	**4606.88**		
18[a]	MEG		Na^+	SO_4^-	**2.25441**	**790.773**		
	Na^+	SO_4^-	MEG		**6.70104**	**0.0789389**		
19[a]	MEG		Na^+	HSO_4^-	**−9**			
	Na^+	HSO_4^-	MEG		**11**			
20[a]	MEG		NH_4^+	SO_4^-	**3.60401**	**408.451**	**48.5586**	
	NH_4^+	SO_4^-	MEG		**−2.90817**	**4.48951**	**−17.1486**	
21[a]	MEG		NH_4^+	HSO_4^-	**1.16708**			
	NH_4^+	HSO_4^-	MEG		**0.000642281**			

[a]Newly obtained interaction parameters.

dosed into the system, and after completing solvent addition, stirring was continued to induce crystal growth. The solids of Na_2SO_4 and $(NH_4)_2SO_4$ were then filtered to obtain samples for SEM and XRD characterization (Figure 11a,b). Figure 11 shows that the two sulfate crystals were obtained in the form of large blocks that have good filtration properties for easy recycling with an average particle size of about 100 μm.

In a continuous process, the concentration of $(NH_4)_2SO_4$ will gradually increase as the crystallization proceeds. The $(NH_4)_2SO_4$ thus needs to be crystallized out to achieve adequate separation of the two inorganic salts. In the experiment reported here, the filtrate from Na_2SO_4 precipitation was cooled to room temperature by vacuum evaporation to induce the crystallization of $(NH_4)_2SO_4$. Evaporative cooling crystallization maintained the water balance throughout the process. Figure 11b shows the shape of the ammonium sulfate crystals produced in the experiment—particle sizes are on the order of 150 μm.

In another set of experiments, the conventional Mirabilite-Solvay process (MSP) was run using our previously crystallized Na_2SO_4 as a raw material. The $NaHCO_3$ was precipitated by purging carbon dioxide into the ammonia-saturated Na_2SO_4 solution in a small column reactor at 323 K. Three SEM photographs of the products are shown in Figure 12. Figure 12a shows $NaHCO_3$, Figure 12b shows $Na_2CO_3.H_2O$ crystallized from concentrated Na_2CO_3 solution, and Figure 12c shows the final dense anhydrous Na_2CO_3 with a bulk density of up to 1146 kg/m^3, which satisfies the Chinese National Standard of 900 kg/m^3.

In order to evaluate the process, a simple mass balance was performed for producing 1 Mt/a Na_2CO_3 in a soda plant as an example. For this production rate, the following raw materials

https://doi.org/10.1021/acsomega.3c07533
ACS Omega 2024, 9, 1265−1277

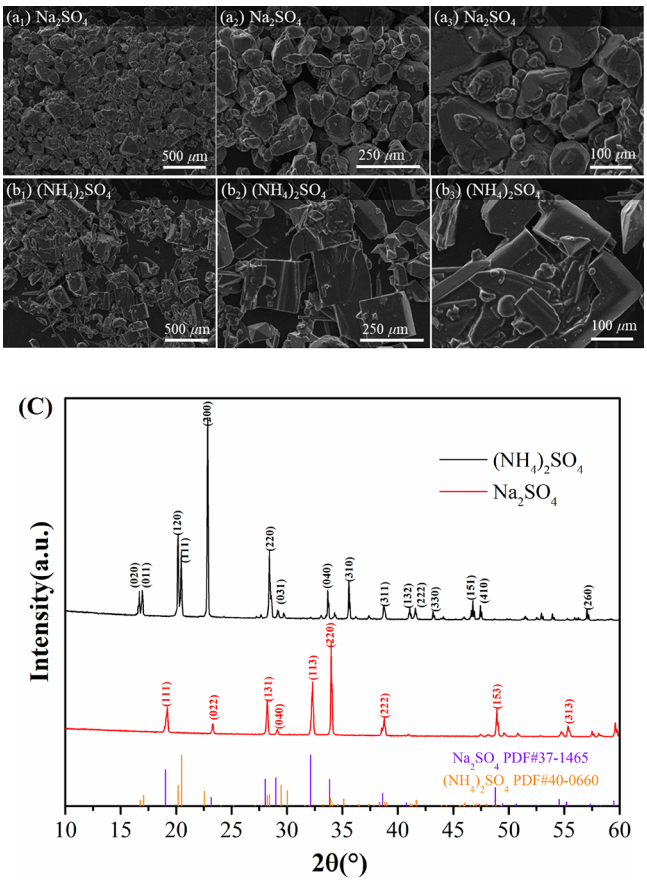

Figure 11. SEM images of Na_2SO_4 (a) and $(NH_4)_2SO_4$ (b) solids obtained using mixed MEA−MEG (50:50) antisolvent crystallization at 353 and 298 K and XRD characterization (c).

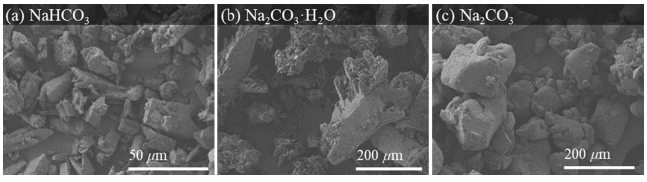

Figure 12. SEM images of $NaHCO_3$(a), Na_2CO_3 H_2O(b) and Na_2CO_3(c) solids obtained using Na_2SO_4 as feed material.

are needed: 1.34 Mt Na_2SO_4, 0.32 Mt NH_3 and 0.415 Mt CO_2. The process makes 1.245 Mt/a of byproduct $(NH_4)_2SO_4$ as saleable fertilizer. It should be noted that the MEA and MEG solvents are not consumed but recycled in the process.

4. CONCLUSIONS

A modified conventional Mirabilite-Solvay Process (MSP) is proposed by incorporating a mixed MEA−MEG antisolvent crystallization step to separate Na_2SO_4 from $(NH_4)_2SO_4$ liquor, in which Na_2CO_3 is produced using Na_2SO_4 as a raw material. This process provides a feasible route for the utilization of sodium sulfate. The following conclusions are obtained from this study:

(1) A newly parametrized E-NRTL activity coefficient model can accurately calculate the solid−liquid equilibrium in the Na_2SO_4−$(NH_4)_2SO_4$−MEA−MEG−H_2O system with Aspen Plus. The thermodynamic model builds on new interaction parameters obtained by regressing the experimental solid−liquid equilibrium data for the $(Na^+\ SO_4^{2-})$:$(NH_4^+\ SO_4^{2-})$, $(Na^+\ SO_4^{2-})$:MEA, $(NH_4^+\ SO_4^{2-})$:MEA, $(Na^+\ SO_4^{2-})$:MEG, $(Na^+\ HSO_4^-)$:MEG, $(NH_4^+\ SO_4^{2-})$:MEG and $(NH_4^+\ HSO_4^-)$:MEG pairs. The total average mole fraction (x) errors are less than 0.015.

(2) The addition of MEG reduces the MEA vapor pressure in aqueous solution and results in less evaporative loss when antisolvent crystallization operates at elevated temperatures. Furthermore, the reduced concentration of MEA in solution also mitigated the release of ammonia and its degradation.

(3) This new process enables the production of Na_2CO_3 from Na_2SO_4 resources and provides an alternative to the conventional Solvay process that uses NaCl as feed and which generates large amounts of chloride-containing waste liquids and solids. Using Na_2SO_4 as the raw material, anhydrous dense soda (Na_2CO_3) produced in this study possesses adequate quality with a bulk density of up to 1146 kg/m^3.

■ ASSOCIATED CONTENT

Data Availability Statement

All data needed to validate the conclusions in the paper are present in the article.

■ AUTHOR INFORMATION

Corresponding Authors

Edouard Asselin − *Department of Materials Engineering, The University of British Columbia, Vancouver, British Columbia V6T 1Z4, Canada;* orcid.org/0000-0001-9492-4949; Email: edouard.asselin@ubc.ca

Zhibao Li − *Key Laboratory of Green Process and Engineering, Institute of Process Engineering, Chinese Academy of Sciences, Beijing 100190, China;* orcid.org/0000-0002-5737-1289; Email: zhibaoli@ipe.ac.cn

Author

Binghui Li − *Department of Materials Engineering, The University of British Columbia, Vancouver, British Columbia V6T 1Z4, Canada*

Complete contact information is available at: https://pubs.acs.org/10.1021/acsomega.3c07533

Author Contributions

B.L.: Solubility determination; data regression; writing−original draft. E.A.: Data curation (supporting), formal analysis; methodology (supporting); writing-review and editing. Z.L.: Project administration; investigation; writing-original draft.

Notes

The authors declare no competing financial interest.

■ ACKNOWLEDGMENTS

Authors are grateful for the financial support provided by the National Science Foundation of China (Grants 21506218).

■ REFERENCES

(1) Garrett, D. E. *Sodium Sulfate: Handbook of deposits, processing, and use*, 1th ed.; Academic Press: London, 2001.

(2) Kostick, D. S. Sodium Sulfate. In *U.S. Geological Survey Minerals Yearbook*; 2013; pp 150−151.

(3) Tan, C.; Wang, A.; Cao, D.; et al. Unravelling the complex Na_2CO_3 electrochemical process in rechargeable Na-CO_2 batteries. *Adv. Energy Mater.* **2023**, *13* (13), No. 2204191.

(4) Zhao, J.; Zhou, F.; Wang, H.; et al. Recovery of lithium iron phosphate batteries through electrochemical oxidation in Na_2CO_3 solutions. *J. Power Sources* **2023**, *582*, No. 233562.

(5) Bolen, W. P. Soda Ash. In *U.S. Geological Survey Minerals Yearbook*; 2020; pp 152−153.
(6) Bi, J.; Shen, R.; Sun, M.; Guo, X.; et al. A continuous electrodialysis metathesis integrated with in-situ CO_2 utilization for controllable $NaHCO_3/NH_4Cl$ or Na_2CO_3/NH_4Cl production from NaCl and $NH_3{\cdot}H_2O$. *Chem. Eng. Sci.* **2024**, *283*, No. 119381.
(7) Gilliard, P.et al.Process for recovering soda values from underground soda deposits. US Patent US9528361 B2, 2016.
(8) Wang, Q.; Li, Z. A modified Solvay process with low-temperature calcination of $NaHCO_3$ using monoethanolamine: solubility determination and thermodynamic modeling. *AlChE J.* **2019**, *65* (10), No. e16701.
(9) Phinnery, R.; Hantke, J. Method of ammonium sulfate purification. US Patent US6106796, 2000.
(10) Bichel, J.; Stephen, S. Method for recovering sodium bicarbonate and ammonium sulfate. US Patent US0156775A1, 2004.
(11) Cisternas, L. A.; Vásquez, C. M.; Swaney, R. E. On the design of crystallization-based separation processes: Review and extension. *AlChE J.* **2006**, *52* (5), 1754−1769.
(12) Gartner, R. S.; Witkamp, G. J. Mixed solvent reactive recrystallization of trona (sodium sesqui-carbonate) into soda (sodium carbonate anhydrate). *Hydrometallurgy* **2007**, *88* (1−4), 75−91.
(13) Ramezani, R.; Mazinani, S.; Di Felice, R. A comprehensive kinetic and thermodynamic study of CO_2 absorption in blends of monoethanolamine and potassium lysinate: experimental and modeling. *Chem. Eng. Sci.* **2019**, *206*, 187−202.
(14) Liu, H.; Li, M.; Luo, X.; Liang, Z.; Idem, R.; Tontiwachwuthikul, P. Investigation mechanism of DEA as an activator on aqueous MEA solution for postcombustion CO_2 capture. *AlChE J.* **2018**, *64* (7), 2515−2525.
(15) Li, B.; Zhang, X.; Li, Z. Phase diagram for the Na_2SO_4−$(NH_4)_2SO_4$−MEA−H_2O system at elevated temperature. *J. Chem. Eng. Data* **2021**, *66*, 3012−3019.
(16) Heldebrant, D. J.; Koech, P. K.; Glezakou, V. A.; Rousseau, R.; Malhotra, D.; Cantu, D. C. Water-lean solvents for post-combustion CO_2 capture: fundamentals, uncertainties, opportunities, and outlook. *Chem. Rev.* **2017**, *117*, 9594−9624.
(17) Puxty, G.; Conway, W.; Botma, H.; Feron, P.; Maher, D.; Wardhaugh, L. A new CO_2 absorbent developed from addressing benzylamine vapour pressure using co-solvents. *Energy Procedia.* **2017**, *114*, 1956−1965.
(18) Neerup, R.; Kloth, D. S.; Almeida, S.; Jørsboe, J. K.; Villadsen, S. N. B.; Fosbøl, P. L. Solid-liquid equilibria of a 30 wt% aqueous monoethanolamine solution containing urea and monoethylene glycol. *J. Chem. Eng. Data* **2021**, *66*, 1231−1237.
(19) Moura-Neto, M. H.; Monteiro, M. F.; Deus, M. S.; Deus, K. C. O.; Oliveira, J. A. F.; Pereira, L. S.; Chiavone-Filho, O. Salt solubility modeling in mixed solvents with a modified Pitzer approach: application in water MEG + electrolyte systems. *AIChE J.* **2023**, *69*, No. e17915, DOI: 10.1002/aic.17915.
(20) Wang, P. M.; Kosinski, J. J.; Anderko, A.; Springer, R. D.; Lencka, M. M.; Liu, J. Ethylene glycol and its mixtures with water and electrolytes: thermodynamic and transport properties. *Ind. Eng. Chem. Res.* **2013**, *52* (45), 15968−15987.
(21) Lencka, M. M.; Kosinski, J. J.; Wang, P.; Anderko, A. Thermodynamic modeling of aqueous systems containing amines and amine hydrochlorides: application to methylamine, morpholine, and morpholine derivatives. *Fluid Phase Equilib.* **2016**, *418*, 160−174.
(22) Jariwala, M.; Crawford, J.; LeCaptain, D. J. In situ raman spectroscopic analysis of the regeneration of ammonium hydrogen sulfate from ammonium sulfate. *Ind. Eng. Chem. Res.* **2007**, *46* (14), 4900−4905.
(23) van der Merwe, E. M.; Gray, C. L.; Castleman, B. A.; Mohamed, S.; Kruger, R. A.; Doucet, F. J. Ammonium sulphate and/or ammonium bisulphate as extracting agents for the recovery of aluminium from ultrafine coal fly ash. *Hydrometallurgy* **2017**, *171*, 185−190.
(24) Douceta, F. J.; Mohamedab, S.; Neytb, N.; Castlemanb, B. A.; van der Merweb, E. M. Thermochemical processing of a South African ultrafine coal fly ash using ammonium sulphate as extracting agent for aluminium extraction. *Hydrometallurgy* **2016**, *166*, 174−184.
(25) Liu, S.; Asselin, E.; Li, Z. Preparation of α-high strength hemihydrate from flue gas desulfurization gypsum in $AlCl_3$-$MgCl_2$ solution at atmospheric pressure. *Ind. Eng. Chem. Res.* **2022**, *61* (37), 14110−14120.
(26) Feldmann, T.; Demopoulos, G. P. Influence of impurities on crystallization kinetics of calcium sulfate dihydrate and hemihydrate in strong HCl-$CaCl_2$ solutions. *Ind. Eng. Chem. Res.* **2013**, *52* (19), 6540−6549.
(27) ASPEN. *Physical Property System (version 8.8)*; ASPEN Technology Inc.: Burlington, MA, 2023.
(28) Tanveer, S.; Chen, C. C. A comprehensive thermodynamic model for high salinity produced waters. *AlChE J.* **2022**, *66* (1), No. e16818.
(29) Yan, Y.; Chen, C. C. Thermodynamic representation of the NaCl + Na_2SO_4+H_2O system with electrolyte NRTL model. *Fluid Phase Equilib.* **2011**, *306*, 149−161.
(30) Raymond, E. V.; Thompson, A. R. Solubility and density isotherms for sodium sulfate−ethylene glycol−water. *Ind. Eng. Chem. Res.* **1949**, *41* (10), 2242−2247.

https://doi.org/10.1021/acsomega.3c07533
ACS Omega 2024, 9, 1265−1277